Center for Turbulence Research
Proceedings of the Summer Program 2006

Implicit subgrid-scale modeling for the large-eddy simulation of passive-scalar mixing

By S. Hickel †, N. A. Adams AND N. N. Mansour

Further development of Large-Eddy Simulation (LES) faces as major obstacles the strong coupling between subgrid-scale (SGS) modeling and the truncation error of the numerical discretization. One can exploit this link by developing discretization methods where the truncation error itself functions as an implicit SGS model. The term implicit LES is used to indicate approaches that merge SGS model and numerical discretization.

In this paper, the implicit SGS modeling environment provided by the Adaptive Local Deconvolution Method (ALDM) is extended to LES of passive-scalar mixing. The resulting method is discussed with respect to its numerical and turbulence-theoretical background. We demonstrate that implicit LES allows for reliable predictions of the turbulent transport of passive scalars in isotropic turbulence and in turbulent channel flow for a wide range of Schmidt numbers.

1. Introduction

Subgrid-scale (SGS) models for Large-Eddy Simulation (LES) generally operate on a range of scales that is marginally resolved by the underlying discretization scheme. Accordingly, the SGS model and the discretization scheme are linked. Ghosal (1996) analyzed this problem and found that the truncation error even of a fourth-order accurate central-difference discretization can have the same order of magnitude as the SGS stress. Kravchenko and Moin (1997) corroborated these theoretical results by numerical simulations.

On the other hand, the interference of SGS model and truncation error can be exploited. With implicit LES the truncation error of the discretization scheme itself is employed to model the effects of unresolved scales, instead of an explicit computation of the SGS stress tensor. Implicit LES can be approached in many ways; a comprehensive review is presented by Grinstein *et al.* (2007). Mostly, given non-linearly stable discretizations schemes for the convective fluxes are used as the main element of implicit SGS models. A numerical analysis of Garnier *et al.* (1999), however, leads to the conclusion that the application of off-the-shelf upwind, variation-limited, or non-oscillatory schemes is not recommended. For the investigated schemes, small scales suffer from excessive numerical damping such that the probability-density functions of velocity increments and pressure exhibit the typical behavior of low Reynolds-number flows rather than that of high Reynolds number turbulence. Thus it appears that for these schemes the prediction accuracy of subgrid effects is poor, although some general trends were reproduced. A more recent review by Grinstein and Fureby (2004), however, emphasizes the potential of implicit LES for physically complex flows and for flows in complex geometries.

Using implicit LES for prediction requires discretization schemes that are specially designed, optimized, and validated for the differential equation to be solved. In order to

† Institute of Aerodynamics, Technische Universität München, 85747 Garching, Germany. E-mail: sh@tum.de

avoid conjecture-based schemes, we have recently developed a systematic framework for implicit LES based on deconvolution methods (Adams *et al.* 2004; Hickel *et al.* 2006*a*). The resulting so-called *Adaptive Local Deconvolution Method* (ALDM) represents a full merging of numerical discretization and SGS model.

ALDM has proven itself as a reliable, accurate, and efficient method for LES. Predictions of ALDM agree well with theory and experimental data. Various applications, e.g. to three-dimensional homogeneous isotropic turbulence (Hickel *et al.* 2006*a*), to plane channel flow (Hickel *et al.* 2005), and to the separated flow in a channel with periodic restrictions (Hickel *et al.* 2006*b*), demonstrate the good performance of the implicit model. It has been shown that the implicit SGS model performs at least as well as established explicit models. This is possible because physical SGS modeling approaches are incorporated into the design of the discretization scheme; in other words, because discretization effects are fully taken into account within the SGS model formulation. Whereas previous approaches to implicit SGS modeling employed available discretization schemes, ALDM is successful because it is optimized for LES of turbulent flows governed by the incompressible Navier-Stokes equations. Other applications require adaptations of the method.

In this paper, our implicit modeling methodology is extended to LES of passive-scalar mixing. We demonstrate that optimized discretization schemes for other differential equations can be derived in the same framework as ALDM. Specific problems in LES of the turbulent transport of passive scalars are addressed in Section 2. The new implicit model is derived, analyzed, and optimized in Sections 3 and 4. Based on the experience with ALDM, where modeling parameters were derived from homogeneous turbulence, we essentially focus on freely decaying three-dimensional homogeneous isotropic turbulence. In Section 6 we report on the application of the new adaptive advection algorithm to the scalar transport in turbulent channel flow, demonstrating that the implicit model correctly predicts mean flow and turbulence statistics for a flow configuration exhibiting anisotropic and inhomogeneous turbulence.

2. The passive-scalar transport equation

A broad range of scientific and engineering applications demonstrate the importance of reliable predictions of the filtered-scale dynamics of scalar quantities that are transported and mixed in turbulent flow. We consider the turbulent transport of *passive* scalars, which do not measurably affect the flowfield. This case represents a one-way coupling of the scalar to the fluid velocity. Hence, the closure problem is restricted to the scalar transport equation. The discretization of the momentum equations remains unchanged.

The transport of a passive scalar c in an incompressible fluid is governed by

$$\partial_t c + \nabla \cdot \boldsymbol{F}(\boldsymbol{u}, c) = 0 \ , \tag{2.1}$$

supplemented with appropriate initial and boundary conditions. The scalar flux function is

$$\boldsymbol{F}(\boldsymbol{u}, c) = \boldsymbol{u}c - \frac{1}{\mathrm{ScRe}} \nabla \ c \ , \tag{2.2}$$

where $\boldsymbol{u}$ and Re are velocity vector and Reynolds number of the transporting flowfield. Sc is the Schmidt number associated with the scalar quantity c. Depending on the application, c can be concentration, temperature, or any kind of passive marker.

Following Leonard (1974), the discretized equation is obtained by convolution with a homogeneous filter kernel G:

$$\partial_t \overline{c} + G * \nabla \cdot \boldsymbol{F}(\boldsymbol{u}, c) = 0 \tag{2.3}$$

and subsequent discretization of the filtered equations

$$\partial_t \overline{c}_N + G * \nabla \cdot \boldsymbol{F}_N(\boldsymbol{u}_N, c_N) = G * \nabla \cdot \boldsymbol{\tau}_{SGS} \ . \tag{2.4}$$

The overbar denotes the filtering $\overline{c} = G * c$ and the subscript N indicates grid functions obtained by projecting continuous functions onto a numerical grid.

The flux (2.2) is formally linear in c. However, the evolution of a non-uniform scalar field is subject to the velocity dynamics. The advection velocity is not constant but varies in time and space. Small-scale fluctuations of velocity and scalar are correlated in the presence of a large-scale scalar-concentration gradient. The problem therefore becomes non-linear. The subgrid tensor

$$\boldsymbol{\tau}_{SGS} = \boldsymbol{F}(\boldsymbol{u}, c) - \boldsymbol{F}_N(\boldsymbol{u}_N, c_N) \tag{2.5}$$

originates from the grid projection of non-linear terms and has to be approximated by a SGS model for closing Eq. (2.4). This modeling task is far from being trivial. One reason is that the various regimes that exist for the passive-scalar variance spectrum have to be recovered by the SGS model. These regimes originate in the difference between typical length scales characterizing the viscous cutoff of the velocity field and the diffusive range of the scaler field. In the following, two regimes that are of particular interest in LES are discussed for homogeneous, isotropic turbulence.

The scalar fluctuations are driven by the stirring induced by the velocity field. Different scalar-transport regimes are associated with certain ranges of Reynolds and Schmidt numbers. The first regime is associated with small Schmidt numbers $\mathrm{Sc} = \nu/\kappa \approx 1$, i.e., the diffusivity κ is close to the viscosity ν. An important application with $\mathrm{Sc} \approx 1$ is the distribution of pollutants in air. With respect to LES, this regime is most relevant at high Reynolds numbers, where the grid size is typically chosen in such a way that the numerical cutoff wavenumber ξ_c is within the inertial range

$$E(\xi) = C_K \varepsilon^{2/3} \xi^{-5/3} \tag{2.6}$$

of the kinetic-energy spectrum. The corresponding scalar-variance spectrum depends on the kinetic-energy transfer ε and is proportional to the scalar diffusion χ. It develops an inertial-convective range

$$E_c(\xi) = C_{OC} \varepsilon^{-1/3} \chi \xi^{-5/3} \tag{2.7}$$

with scaling $E_c(\xi) \sim \xi^{-5/3}$. C_K and C_{OC} are Kolmogorov constant and Obukhov-Corrsin constant.

A more complex situation is encountered if the Schmidt number is much larger than unity $\mathrm{Sc} \gg 1$. In this regime two distinct inertial ranges exist for the scalar-variance spectrum. An inertial-convective range (2.7) is observed for scales within the Kolmogorov inertial range of the kinetic-energy spectrum. At smaller scales, the scalar fluctuations are not yet affected by diffusion, whereas the energy spectrum already decays exponentially. A second inertial range, the viscous-convective range, is observed for the scalar variance driven by a time scale, e.g. $(\nu/\varepsilon)^{1/2}$, of the stirring motion of the velocity field. In the viscous-convective range, the scalar variance spectrum

$$E_c(\xi) = C_B \nu^{1/2} \varepsilon^{-1/2} \chi \xi^{-1} \ . \tag{2.8}$$

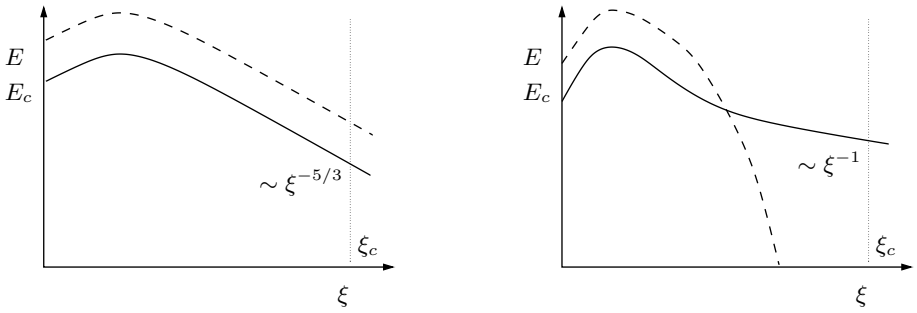

FIGURE 1. Critical test cases for predicting the proper subgrid diffusion in large-eddy simulations of scalar mixing. *Left:* Low Schmidt number regime. *Right:* High Schmidt number regime at moderate Reynolds number. ——— scalar variance ; – – – – kinetic energy.

exhibits a ξ^{-1} scaling. If the grid width lies within the inertial-convective range, the same SGS modeling can be used as for the Sc ~ 1 case. A different approach is required if the numerical cutoff is chosen within the viscous-convective range. This velocity-resolving case is typically associated with low Reynolds numbers in LES.

In summary, two critical test cases are identified for SGS modeling representing different physical regimes of passive-scalar mixing in isotropic turbulence. Generic sketches of corresponding kinetic energy spectra, scalar variance spectra, and numerical cutoff are shown in Fig. 1.

Another difficulty in solving scalar transport equations is associated with a numerical problem. At high Schmidt numbers, even an incompressible and smooth flowfield will generate a filtered scalar field with steep concentration gradients that can only be captured and not resolved by the numerical discretization. Standard centered differencing schemes tend to non-physical oscillations unless they are supplemented with a numerical regularization.

3. Discretization design

Previous approaches to implicit LES mostly rely on trial and error. Suitable schemes with physical relevance were found by merely guessing. We have developed a framework for a more systematic approach to implicit SGS modeling.

First, a general non-linear discretization scheme with an unknown but adjustable truncation error is designed. Such a scheme usually combines standard approaches. These, however, have to be modified in such a way that the numerical truncation error can be controlled through inherent parameters. The resulting scheme should be as simple as possible to facilitate computation at reasonable cost, yet as complex as necessary to allow for implicit modeling. In a second step, this general method is analyzed with respect to its implicit SGS modeling capabilities. Finally, appropriate values of the parameters inherent to the discretization scheme are determined in such a way that the truncation error of the method acts as a physical SGS model. For a comprehensive description of methods for design, analysis, and optimization of discretization schemes, see Hickel *et al.* (2006*a*) and references therein.

The truncation error of a general discretization scheme can be written as

$$\mathcal{G}_N = G * \nabla \cdot \boldsymbol{F}_N(\boldsymbol{u}_N, c_N) - \widetilde{G} * \widetilde{\nabla} \cdot \widetilde{\boldsymbol{F}}_N(\widetilde{\boldsymbol{u}}_N, \widetilde{c}_N) \ , \tag{3.1}$$

where a tilde indicates the respective numerical approximation. For example, the unfil-

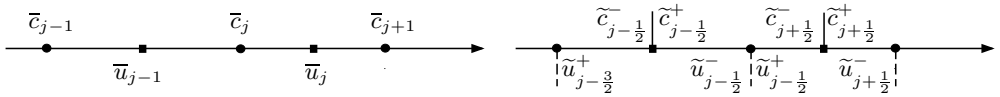

FIGURE 2. Staggered grid arrangement. *Left:* Filtered solution. *Right:* Reconstructions of unfiltered solution in a finite volume discretization.

tered, i.e., continuous, solution c is unknown in an LES. However, an approximation $\widetilde{c}_N$ of the grid function c_N can be obtained from $\overline{c}_N$ by regularized deconvolution (Domaradzki and Adams 2002). Hence, the solution $\overline{c}_N$ obtained with the discrete operators does not satisfy Eq. (2.4), but rather a modified differential equation (MDE). This is exploited in implicit LES where no subgrid tensor is computed and the MDE becomes

$$\partial_t \overline{c}_N + G * \nabla \cdot \boldsymbol{F}_N(\boldsymbol{u}_N, c_N) = \mathcal{G}_N \ . \tag{3.2}$$

The numerical truncation error can act as an implicit SGS model. Particularly, an explicit SGS model is resembled if the filtered divergence of the model SGS tensor is approximated

$$\mathcal{G}_N \approx -G * \nabla \cdot \boldsymbol{\tau}_{SGS} \ . \tag{3.3}$$

The most suitable framework for implicit LES is provided by the finite-volume method. The truncation error of finite-volume methods readily appears in the form of a divergence of a tensor. This is advantageous with respect to physically motivated implicit modeling. A finite-volume discretization corresponds to the evaluation of Eq. (2.4) with the tophat filter kernel

$$G(x - x_j, h) = \begin{cases} 1/h & , \ |x - x_j| \leq h/2 \\ 0 & , \ \text{else} \end{cases} \tag{3.4}$$

on a computational grid $x_N = \{x_j\}$. For brevity of notation and without loss of generality, the following derivation is given for the one-dimensional case. The three-dimensional scheme is obtained in a similar manner to the simplified adaptive deconvolution (SALD) method (Hickel and Adams 2006*a*,*b*). A staggered arrangement of velocity, pressure, and scalar (see Fig. 2) is used to allow for an accurate and stable solution of the pressure-Poisson equation in 3-D incompressible flows.

Following Schumann (1975), a finite-volume discretization implies reconstruction of the unfiltered solution at cell faces and the approximation of the physical flux function by a numerical flux function. Deconvolution and interpolation can be done simultaneously using Lagrangian approximation polynomials

$$\widetilde{p}^{\mp}_{k,r}(\overline{\phi}_N) = \sum_{l=0}^{k-1} \alpha^{\mp}_{k,r,l}(x_N)\overline{\phi}_{j-r+l} \ , \tag{3.5}$$

as proposed by Harten *et al.* (1987). Half-integer indices denote reconstructions at the cell faces. The grid-dependent coefficients $\alpha^{\mp}_{k,r,l}$ are chosen such that

$$\widetilde{p}^{\mp}_{k,r}(\overline{\phi}_N) = \phi(x_{j\pm1/2}) + \mathcal{O}\left(h^k\right) \ . \tag{3.6}$$

With implicit LES we do not aim at the formally highest order of accuracy. Instead, deconvolution is regularized by limiting the degree K of local approximation polynomials and by permitting lower-order polynomials $1 \leq k < K$ to contribute to the approximately deconvolved solution

$$\widetilde{u}^{\mp}_{j\pm1/2} = \sum_{k=1}^{K}\sum_{r=0}^{k-1} \omega^{\mp}_{k,r}(\overline{u}_N)\widetilde{p}^{\mp}_{k,r}(\overline{u}_N) \quad , \qquad \widetilde{c}^{\mp}_{j\pm1/2} = \sum_{k=1}^{K}\sum_{r=0}^{k-1} \omega^{\mp}_{k,r}(\overline{c}_N)\widetilde{p}^{\mp}_{k,r}(\overline{c}_N) \ . \tag{3.7}$$

Explicit SGS modeling has clearly demonstrated the benefits of dynamic, solution-adaptive strategies. Adaptivity of the reconstruction scheme is achieved by weighting the contributions of different polynomial approximants. The weights

$$\omega_{k,r}^{\pm}\left(\overline{\phi}_N\right) = \frac{1}{K}\frac{\gamma_{k,r}^{\pm}\beta_{k,r}\left(\overline{\phi}_N\right)}{\sum_{s=0}^{k-1}\gamma_{k,s}^{\pm}\beta_{k,s}\left(\overline{\phi}_N\right)} \tag{3.8}$$

are constructed from a non-linear function $\beta_{k,r}\left(\overline{\phi}_N\right)$ of the solution that measures the smoothness within the respective stencil (see Hickel *et al.* 2006*a*). Free parameters $\gamma_{k,r}^{-} = \gamma_{k,r}$ and $\gamma_{k,r}^{+} = \gamma_{k-r-1,r}$ inherent to these weight functions represent a stencil-selection preference that would become effective in the statistically homogeneous case. The approximately deconvolved solution is inserted into a consistent numerical flux function. Based on direct numerical experimentation, we propose

$$\widetilde{F}_N(x_{j\pm1/2}) = F\left(\frac{\widetilde{u}_{j\pm1/2}^{-} + \widetilde{u}_{j-1\pm1/2}^{+}}{2}, \frac{\widetilde{c}_{j\pm1/2}^{-} + \widetilde{c}_{j\pm1/2}^{+}}{2}\right) - \sigma_{j\pm1/2}\left(\widetilde{c}_{j\pm1/2}^{+} - \widetilde{c}_{j\pm1/2}^{-}\right) , \tag{3.9}$$

where $\sigma_{j\pm1/2}$ can be any shift-invariant functional. Note that velocity and scalar are defined at different positions (Fig. 2). The indices are given in specific coordinate systems relative to the original position on a staggered grid. From a dimensional argument, it follows that $\sigma_{j\pm1/2}$ is a velocity. In order to obtain a Galilean invariant discretization, we define

$$\sigma_{j\pm1/2} = \sigma_c\left|\widetilde{u}_{j\pm1/2}^{-} - \widetilde{u}_{j-1\pm1/2}^{+}\right| , \tag{3.10}$$

where σ_c is another free parameter of the discretization.

4. Analysis and optimization

Discretization coefficients are usually chosen in such a way that the formal order of accuracy of the discretization is maximized. This classical approach holds for direct numerical simulations but not for LES, where the grid resolution essentially defines the range of represented scales. At finite grid size, numerical truncation errors interfere with turbulence model and modeling errors. For LES, free discretization coefficients should be chosen such that the sum of all contributions (truncation errors and SGS model terms) acts as a physically relevant SGS model.

With implicit LES, numerical discretization and turbulence model are inseparable. The values of free discretization parameters are determined in such a way that the truncation error of the discretization method acts as a physically motivated SGS model. For this purpose the modified differential equation (MDE) of the discretization method is analyzed. Hickel *et al.* (2006*a*) proposed an *a posteriori* analysis of the spectral numerical dissipation in numerical simulations of freely decaying homogeneous isotropic turbulence. This method follows from the hypothesis that the primary purpose of an SGS model is to provide the correct spectral distribution of subgrid dissipation. A semi-analytical expression for the eddy-viscosity spectrum in isotropic turbulence at high Reynolds numbers is provided by Chollet (1984) based on the eddy-damped quasi-normal Markovian (EDQNM) theory (see Lesieur 1997). A robust automatic optimization procedure based on an evolutionary approach was applied for minimizing a cost function that measures the difference between spectral numerical viscosity of ALDM and the eddy viscosity from

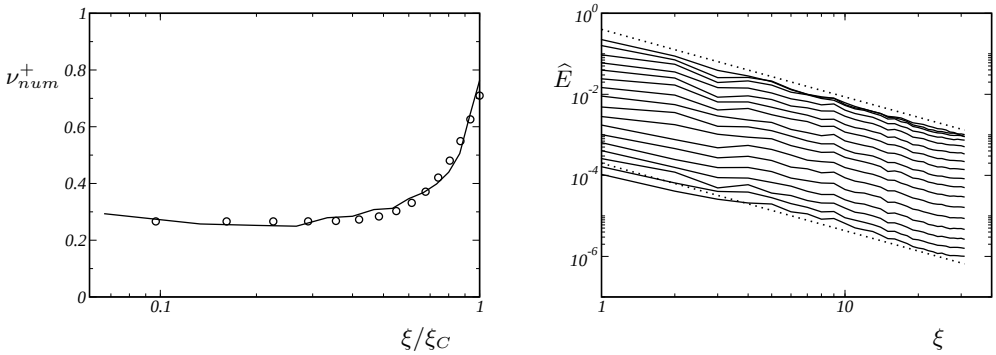

FIGURE 3. Implicit LES of decaying homogeneous isotropic turbulence at the inviscid limit. *Left:* Numerical viscosity of ALDM with optimized parameters compared to the prediction of turbulence theory. ——— implicit LES with ALDM ; ∘ EDQNM theory (Chollet 1984). *Right:* Instantaneous 3-D energy spectra. ——— ALDM ; ····· $\widehat{E} \sim \xi^{-5/3}$.

EDQNM. With the optimized discretization parameters the numerical viscosity matches the theoretical requirements of EDQNM. The eddy-viscosity spectrum of ALDM exhibits a low-wavenumber plateau at the correct level and reproduces the typical cusp shape up to the cutoff wavenumber ξ_C at the correct magnitude (Fig. 3).

In this paper the same approach is taken to optimize the spectral numerical diffusivity of a discretization method for the passive-scalar transport equation. A first analysis indicated that the solution-adaptive deconvolution operator with parameters $\gamma_{k,r}$ is responsible for a sharply rising cusp of the spectral numerical diffusivity at high wavenumbers. The spectral numerical diffusivity due to the flux function is almost constant where the level of the diffusivity can be adjusted by the free parameter σ_c.

We decided to optimize σ_c only while using the same values for $\gamma_{k,r}$ as provided by ALDM for the momentum equation (Hickel *et al.* 2006*a*) due to the lack of a reliable cost function for optimizing the shape of the subgrid diffusivity spectrum $\kappa_{SGS}(\xi)$. An EDQNM analysis leads to the conclusion that $\kappa_{SGS}(\xi)$ is proportional to the spectral eddy viscosity $\nu_{SGS}(\xi)$. However, this finding is questionable because several contradictory results from measurements and direct simulations are given in the literature (see, e.g., Lesieur 1997).

On the other hand, the integral amount of necessary subgrid diffusion can be estimated by a simple analysis. In our test configurations, isotropic turbulence at high Péclet numbers $\mathrm{Pe} = \mathrm{Sc} \cdot \mathrm{Re}$, diffusion is exclusively provided by the SGS model, i.e.,

$$\chi_{SGS} = \chi \ . \tag{4.1}$$

We define the equivalent subgrid diffusivity

$$\overline{\kappa}_{SGS} = \frac{\int \kappa_{SGS}(\xi)\xi^2 E_c(\xi) d\xi}{\int \xi^2 E_c(\xi) d\xi} \ . \tag{4.2}$$

From Eq. (2.6, 2.7, and 4.1) follows

$$\overline{\kappa}_{SGS} = \frac{2}{3} C_{OC}^{-1} \varepsilon^{1/3} \xi_c^{4/3} = \frac{C_K}{C_{OC}} \overline{\nu}_{SGS} \tag{4.3}$$

for the low Schmidt number test case. Assuming identical spectral distributions, the equivalent subgrid diffusivity is obtained from the subgrid viscosity by multiplication with the ratio of Kolmogorov constant and Obukhov-Corrsin constant. Unfortunately,

	$\gamma_{2,0}$	$\gamma_{2,1}$	$\gamma_{3,0}$	$\gamma_{3,1}$	$\gamma_{3,2}$	σ_c
if Sc ≈ 1	1.00000	0.00000	0.01902	0.08550	0.89548	0.61500
if Sc $\gg 1$	1.00000	0.00000	0.01902	0.08550	0.89548	0.30000

TABLE 1. Optimized discretization parameters of passive-scalar ALDM.

measurements for both constants scatter a lot. The Obukhov-Corrsin constant is in the range $0.68 \leq C_{OC} \leq 0.83$ (Sagaut 2005). The range of reported values for the Kolmogorov constant is even wider, most likely within $1.4 \leq C_{OC} \leq 1.8$ (Yeung and Zhou 1997).

Our initial estimate for the proportionality constant in Eq. (4.3) was $C_K/C_{OC} = 2.0$. With parameters optimized accordingly, the scalar-variance spectrum is unsteady. At time instants it can be as flat as ξ^{-1} in LES of low Schmidt number isotropic turbulence. The slope of the mean spectrum is close to $\xi^{-5/3}$ but clearly not steep enough. Numerical experimentation led us to the conclusion that $C_K/C_{OC} \approx 2.3$ is a much better approximation.

The theoretical scalar-variance spectrum in high Schmidt number isotropic turbulence is given in Eq. (2.8). The presence of the viscosity in this equation does not imply that the scalar SGS model has to incorporate the Reynolds number, but rather that $\boldsymbol{\tau}_{SGS}$ depends on the shape of the viscous range. The term $(\nu/\varepsilon)^{1/2}$ can be computed analytically in velocity-resolving simulations. This leads to an exact constraint for the mean eddy-diffusivity

$$\overline{\kappa}_{SGS} = 2\left(\frac{\nu}{\varepsilon}\right)^{-1/2} \xi_c^{-2} \,, \tag{4.4}$$

which has to be met by the implicit SGS model.

Table 1 summarizes the values for the free discretization coefficients that were selected. These parameters are optimized based on an analysis of the numerical diffusivity of the model in simulations of passive-scalar mixing in freely decaying isotropic turbulence. This analysis also revealed that different parameters are required for the two regimes. Hence, two sets of parameters were determined representing two SGS models: one for low Schmidt numbers and one for high Schmidt numbers.

5. Validation for forced isotropic turbulence

The new model is applied in the first test case to passive-scalar mixing in forced isotropic turbulence. An extra source term was added to the right-hand side of the Navier-Stokes equations and the scalar-transport equation. This forcing results in a production of scalar variance and kinetic energy that compensates diffusion and dissipation while preserving the shape of the spectra. By construction, only large scales $|\boldsymbol{\xi}| \leq 2$ are affected by the forcing.

We performed two simulations, one for each scalar-mixing regime. For the low Schmidt number regime, the computational Reynolds numbers $\mathrm{Re} = 1/\nu$ is $\mathrm{Re} = 10^4$ and the Schmidt number is $\mathrm{Sc} = 1$. The high Schmidt number model is tested for Reynolds number $\mathrm{Re} = 20$ and Schmidt number $\mathrm{Sc} = 400$. The grid is composed of 32^3 evenly-spaced cells. For the lower Reynolds number, the Kolmogorov length scale is on the order of the mesh size.

After an initial transient, samples of the 3-D scalar-variance and kinetic-energy spectra were collected until the mean spectra were converged. The resulting 3-D mean spectra are

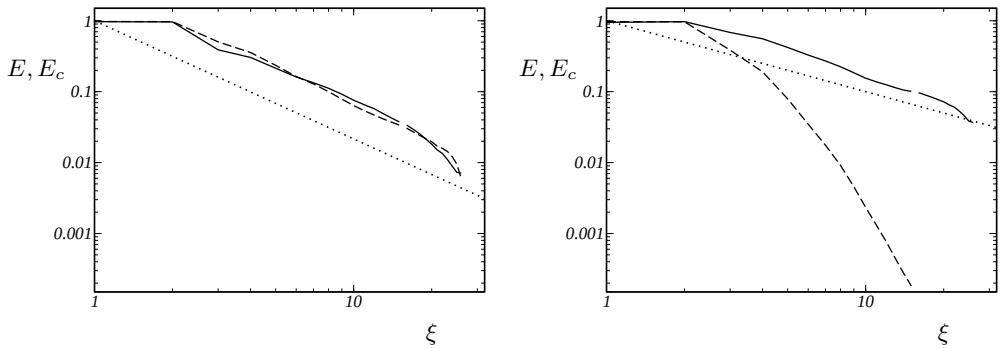

FIGURE 4. Mean 3-D spectra of kinetic energy and scalar variance for implicit LES of large-scale forced isotropic turbulence. *Left:* $\mathrm{Re} = 10^4$ and $\mathrm{Sc} = 1$. *Right:* $\mathrm{Re} = 20$ and $\mathrm{Sc} = 400$. ——— scalar variance; – – – – kinetic energy; ····· analytical expressions for scalar variance.

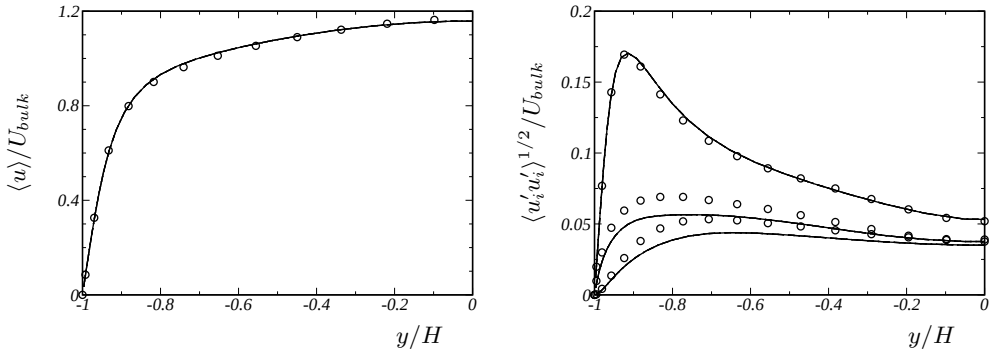

FIGURE 5. Mean velocity profile and Reynolds stresses in turbulent channel flow at $\mathrm{Re}_\tau = 180$. ——— implicit LES with SALD, ∘ DNS data of Moser *et al.* (1999).

shown in Fig. 4. A small gap in the lines marks the wavenumber $\xi_c = 15$. Wavenumbers $\xi_c < |\boldsymbol{\xi}| < \sqrt{3}\xi_c$ are only partially represented in physical-space simulations. Both simulations agree reasonably well with the expected solution. This result verifies *a posteriori* the parameter selection which was based on the corresponding theoretical prediction.

6. Application to turbulent channel flow

6.1. *Test case and computational setup*

Reliable reference data are very rare for flows at higher Schmidt numbers. Most SGS models for scalar transport have been validated only for $\mathrm{Sc} < 1$ since DNS of developed turbulent flows at Schmidt numbers $\mathrm{Sc} \gg 1$ have only recently become feasible. Today, such DNS are still limited to very moderate Reynolds numbers. Schwertfirm and Manhart (2006) performed DNS of the transport of passive scalars in turbulent channel flow at Reynolds number $\mathrm{Re}_\tau = 180$ and at Schmidt numbers $\mathrm{Sc} = 1$, 3, 10, and 25. In order to validate the new method in wall-bounded flows, implicit LES are conducted where computational setup, Reynolds number, and Schmidt numbers are adapted to this reference.

The computational domain is a plane channel that measures $2\pi H \times 2H \times \pi H$ in streamwise, wall-normal, and spanwise direction, respectively. Periodic boundary conditions are

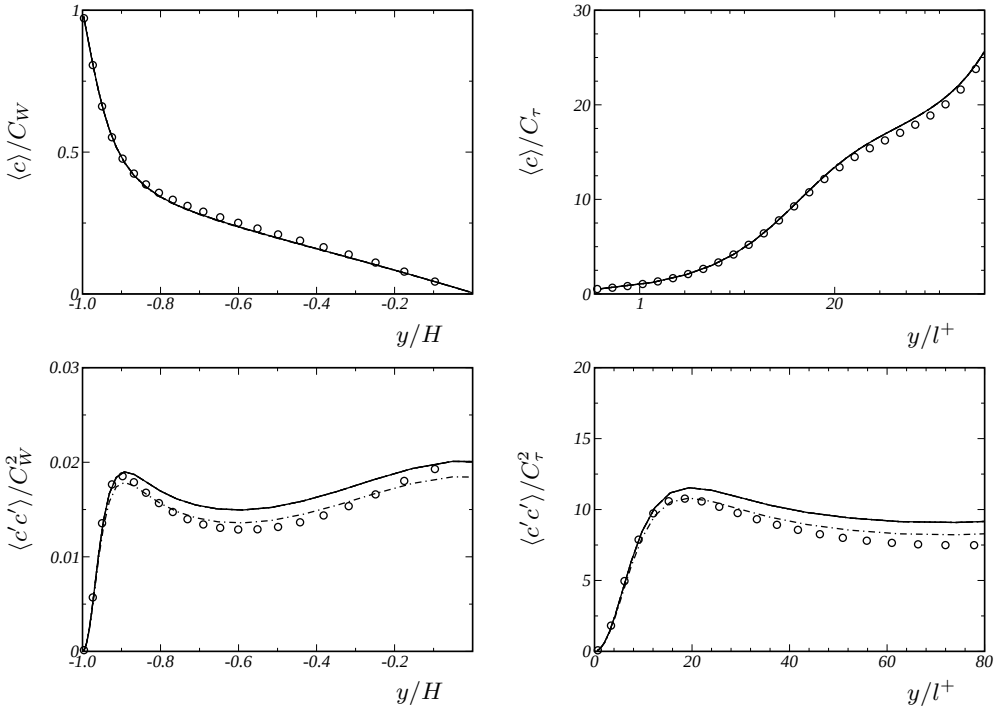

FIGURE 6. Profiles of mean scalar concentration and scalar variance in plane channel flow at $\mathrm{Re}_\tau = 180$ and $\mathrm{Sc} = 1$. Implicit LES with parameters optimized for ——— high Schmidt numbers, ·—·—·— low Schmidt numbers, ∘ DNS of Schwertfirm and Manhart (2006).

imposed in streamwise and spanwise direction. No wall model is used in the simulations, rather the no-slip condition is imposed directly on the velocity field. The scalar is added to the fluid at one wall and removed at the opposite wall, i.e., the wall concentration $C_W = \pm 1$ of the scalar is kept constant.

The computational domain is discretized by $48 \times 48 \times 48$ cells. The grid is stretched in wall-normal direction by the hyperbolic tangent function

$$y(j) = -\frac{H}{\tanh(C_G)} \tanh\left(C_G - 2CG\frac{j}{N_y + 1}\right) \tag{6.1}$$

to accommodate the change of turbulence structure in the vicinity of the walls. N_y is the number of cells in the wall-normal direction and $C_G = 2.5$ is the grid-stretching parameter (c.f. Gullbrand and Chow 2003).

Figure 5 shows mean velocity profile and Reynolds stresses from implicit LES using the SALD method. We observe a good agreement with the reference DNS data. The profiles of higher-order moments show small discrepancies, which are inevitable when comparing DNS with LES on coarser grids. These results show that the grid allows for sufficiently well-resolved LES of the velocity field. Note that similar results for the velocity field can be obtained with fewer grid points than used here. However, it is known that the relative resolution requirement for the scalar field increases with the square root of the Schmidt number. This scaling holds for the Batchelor scale $\eta_B = \eta_K/\sqrt{\mathrm{Sc}}$ (the equivalent of the Kolmogorov η_K scale) and for the thickness of the conductive (diffusive) sublayer.

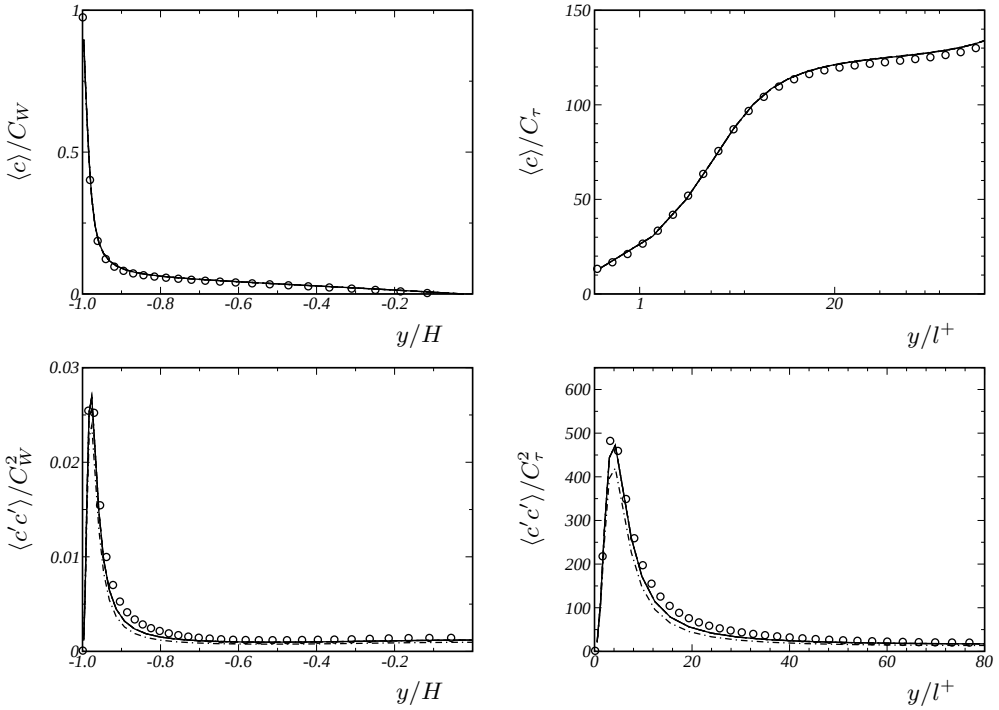

FIGURE 7. Profiles of mean scalar concentration and scalar variance in plane channel flow at $\mathrm{Re}_\tau = 180$ and $\mathrm{Sc} = 25$. Implicit LES with parameters optimized for ——— high Schmidt numbers, ·—·—·— low Schmidt numbers, ∘ DNS of Schwertfirm and Manhart (2006).

proportional to We intend to use the same computational grid for Schmidt numbers between $1 \leq \mathrm{Sc} \leq 25$. As a compromise we chose a grid with 48^3 cells.

6.2. *Scalar statistics*

We performed implicit LES at Schmidt numbers $\mathrm{Sc} = 1$, 3, 10, and 25 using the SALD methods optimized for high and for low Schmidt numbers. Figures 6 and 7 show profiles mean scalar concentration $\langle c\rangle$ and scalar variance $\langle c'c'\rangle$ for implicit LES at $\mathrm{Sc} = 1$ and $\mathrm{Sc} = 25$. Profiles of the turbulent mass transport $\langle c'u'\rangle$ and $\langle c'v'\rangle$ are shown in Fig. 8 and 9. The computational results are normalized with the bulk velocity U_{bulk} and wall concentration C_W or with friction velocity $U_\tau = \nu\langle\partial_y u\rangle$ and friction concentration $C_\tau = \kappa/U_\tau\langle\partial_y c\rangle$.

At both Schmidt numbers, an excellent agreement with the reference DNS data and a close match between both implicit models is observed. The implicit modeling approach gives good predictions for scalar mixing in turbulent channel flow although the model parameters were derived for isotropic turbulence.

For the Schmidt number considered, the role of optimal parameter choice is less important in turbulent channel flow than in isotropic turbulence. Nevertheless, the low Schmidt number scheme gives better predictions at $\mathrm{Sc} = 1$, whereas the high Schmidt number scheme performs slightly better at $\mathrm{Sc} = 25$. Implicit LES at $\mathrm{Sc} = 3$ (not shown) and $\mathrm{Sc} = 10$ (see Fig. 10) show the same tendency as the $\mathrm{Sc} = 25$ case. The results suggest that benefits of the high Schmidt number scheme become more relevant at larger Schmidt numbers.

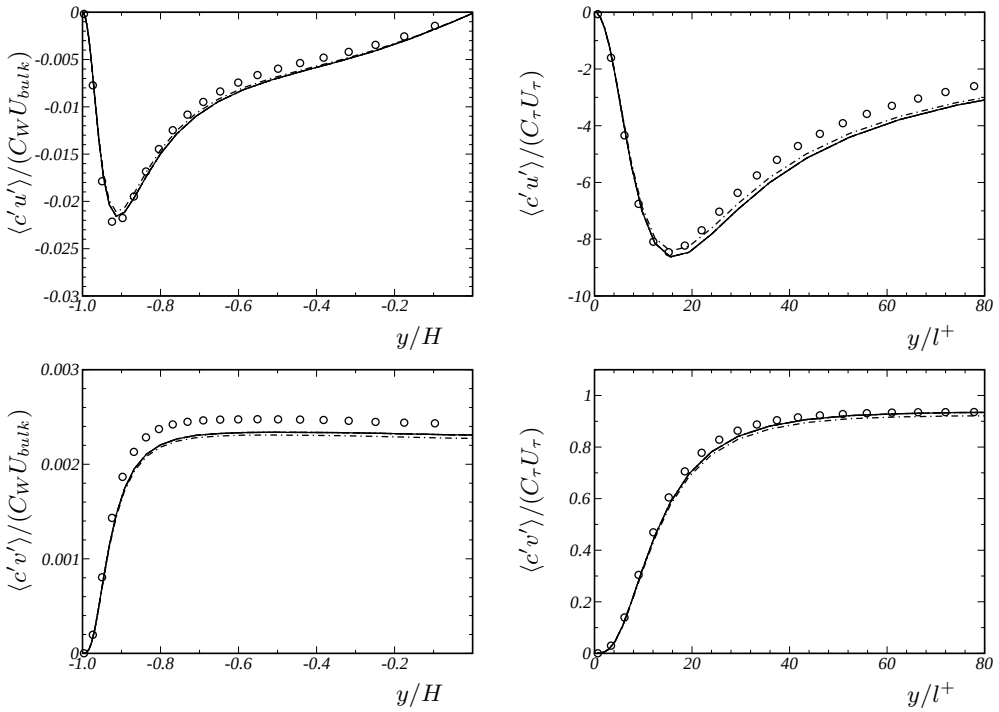

FIGURE 8. Turbulent transport of a passive scalar in plane channel flow at $\mathrm{Re}_\tau = 180$ and $\mathrm{Sc} = 1$. Implicit LES with parameters optimized for ——— high Schmidt numbers, ·—·—·— low Schmidt numbers, ○ DNS of Schwertfirm and Manhart (2006).

6.3. *Grid-convergence study*

The LES presented in the preceding section were performed on identical grids with 48^3 cells. Although this resolution was chosen somewhat arbitrarily, implicit LES using this grid accurately predict the passive-scalar statistics for Schmidt numbers $1 \leq \mathrm{Sc} \leq 25$. However, it is well known that the choice of resolution can significantly alter the results of implicit as well as explicit LES. In the following, the role of resolution is studied qualitatively. The grid convergence of the spatial discretization and the inherent SGS model is evaluated by comparing statistics from implicit LES at different spatial resolutions. It is clear that more quantitative measures are desirable to establish a formal proof of accuracy of a numerical method. Preferably, the accuracy of a discretization scheme is measured in terms of convergence with a certain order toward the exact instantaneous solution.

The investigated method represents a merge between numerical discretization scheme and turbulence model. Analyses of turbulence models are often performed on the basis of pre-computed turbulent solutions to the 3-D Navier-Stokes equations. However, these so called *a priori* analyses suppress the inherent dynamics of an LES and can lead to questionable conclusions concerning the behavior in real simulations. Turbulence models for LES do model the statistical effect on the resolved scales of their non-linear interaction with unknown SGS. Hence, LES cannot aim at the exact reproduction of instantaneous solutions but rather at the accurate prediction of statistical properties of the resolved scales. It can be argued that results from LES should be compared with statistics computed from filtered DNS solutions. However, this would render a grid-convergence study

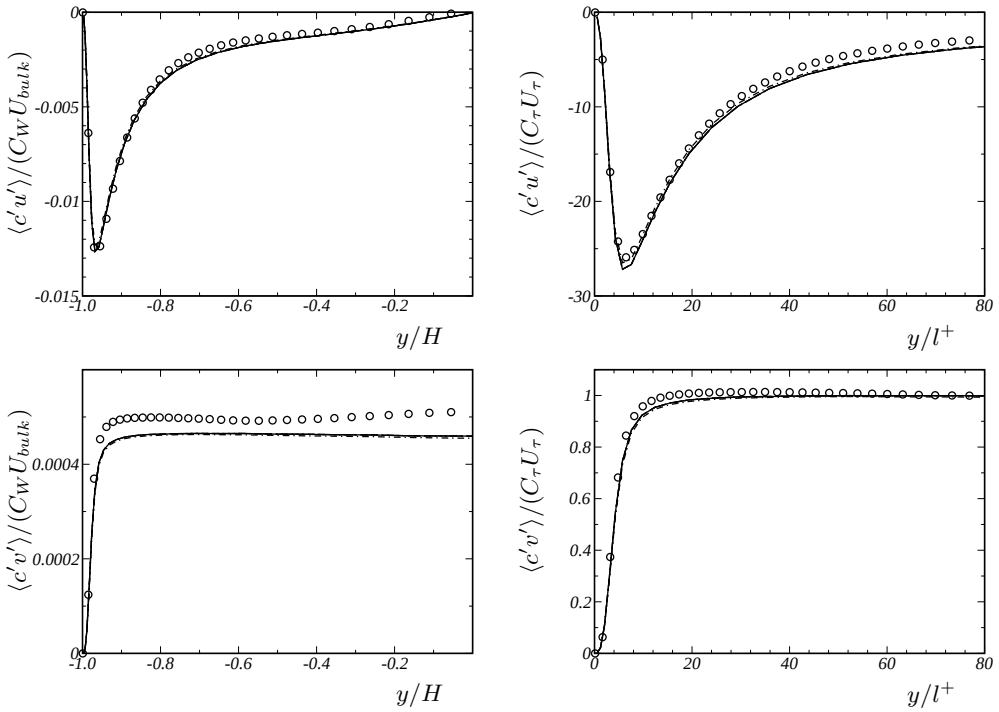

FIGURE 9. Turbulent transport of a passive scalar in plane channel flow at $\mathrm{Re}_\tau = 180$ and $\mathrm{Sc} = 25$. Implicit LES with parameters optimized for ——— high Schmidt numbers, ·—·—·— low Schmidt numbers, ○ DNS of Schwertfirm and Manhart (2006).

impossible since in the presented implicit LES (and in most explicit LES) the filter width is proportional to the grid width. We therefore chose to compare statistics from implicit LES at different spatial resolutions with unfiltered DNS data.

Figure 10 shows profiles of mean scalar concentration, scalar variance, and turbulent transport for DNS and LES of turbulent channel flow at $\mathrm{Re}_\tau = 180$ and $\mathrm{Sc} = 10$. The reference DNS was conducted by Schwertfirm and Manhart (2006) on a grid with $720 \times 300 \times 384$ cells. This data is compared to LES from grids with 24^3, 32^3, 48^3, and 64^3 cells. The results from implicit LES with 64^3 cells are in very close agreement with the reference DNS. All statistics show clear convergence toward the reference solution with an increasing number of grid points. This tendency is most significant for the turbulent mass fluxes, whereas the scalar variance itself is very insensitive to the grid resolution. The larger effect on the turbulent transport can be attributed to similar trends observed in the fluctuations of the transporting velocity components.

In summary, we observe a monotone convergence toward the reference solution. The individually required resolution depends on the required accuracy in the turbulent mass fluxes.

7. Conclusions

We have proposed systematic procedures for design, analysis, and optimization of non-linear discretization schemes for implicit LES. The resulting adaptive local deconvolution method (ALDM) represents a full merging of numerical discretization and SGS model.

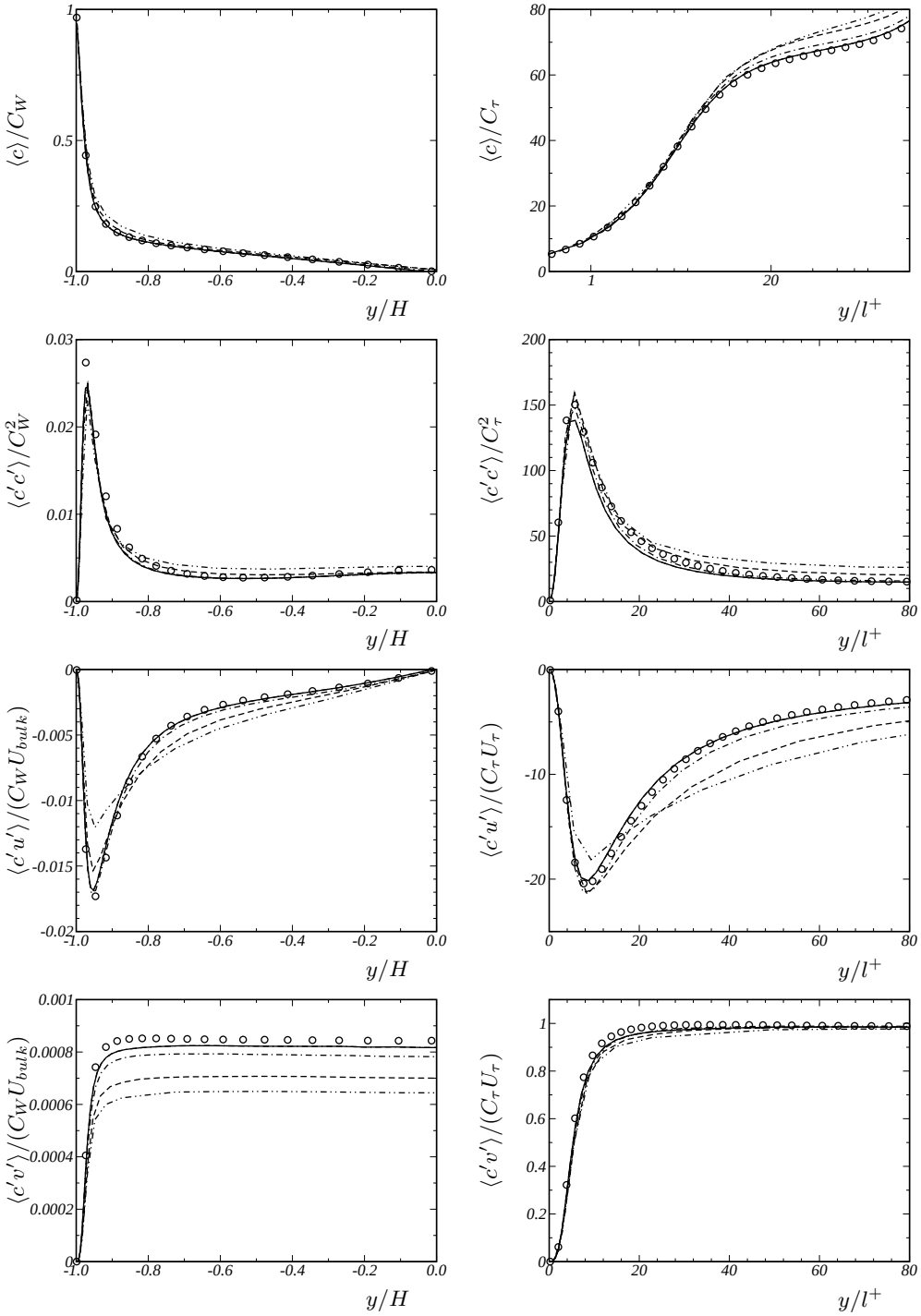

FIGURE 10. Grid-convergence study for implicit LES of passive-scalar transport in turbulent channel flow at $\mathrm{Re}_\tau = 180$ and $\mathrm{Sc} = 10$. Implicit LES using the high Schmidt number SALD method on a grid with ——— 64^3 cells , ·—·—· 48^3 cells , – – – – 32^3 cells —··—··— 24^3 cells. ∘ DNS of Schwertfirm and Manhart (2006)

ALDM provides the first systematic framework for implicit SGS modeling and incorporates the essential elements of LES, filtering and deconvolution.

In the present paper, this implicit SGS modeling environment is extended to LES of passive-scalar mixing. We have developed a non-linear, solution adaptive discretization scheme for the scalar advection equation, which is based on the main numerical building blocks provided by finite-volume discretizations. The effective eddy-diffusivity spectrum of the implicit model inherent in the adaptive advection algorithm was analyzed. Discretization coefficients are determined in such a way that the numerical truncation error acts as a physically motivated SGS model matching the requirements of EDQNM theory in isotropic turbulence. The implicit model combines eddy-diffusivity modeling with a generalized scale-similarity approach.

The choice of discretization model parameters is validated for forced isotropic turbulence. Applications to turbulent channel flow demonstrate that implicit LES allows for reliable predictions of the turbulent transport of passive scalars for a wide range of Schmidt numbers.

Acknowledgments

The authors wish to thank the Center for Turbulence Research at Stanford University for hospitality and financial support. Florian Schwertfirm is gratefully acknowledged for providing reference DNS data for passive-scalar mixing in turbulent channel flow. SH is supported by the German Research Council (Deutsche Forschungsgemeinschaft - DFG) in the framework of the French-German research group FG507.

REFERENCES

Adams, N. A., Hickel, S. & Franz, S. 2004 Implicit subgrid-scale modeling by adaptive deconvolution. *J. Comp. Phys.* **200**, 412–431.

Chollet, J.-P. 1984 Two-point closures as a subgrid-scale modeling tool for large-eddy simulations. In *Turbulent Shear Flows IV* (ed. F. Durst & B. E. Launder), pp. 62–72. Heidelberg: Springer.

Domaradzki, J. A. & Adams, N. A. 2002 Direct modeling of subgrid scales of turbulence in large-eddy simulations. *J. Turb.* **3**, 24.

Garnier, E., Mossi, M., Sagaut, P., Comte, P. & Deville, M. 1999 On the use of shock-capturing schemes for large-eddy simulation. *J. Comput. Phys.* **153**, 273–311.

Ghosal, S. 1996 An analysis of numerical errors in large-eddy simulations of turbulence. *J. Comput. Phys.* **125**, 187–206.

Grinstein, F., Margolin, L. & Rider, W., ed. 2007 *Implicit Large Eddy Simulation: Computing Turbulent Flow Dynamics*. Cambridge, UK: Cambridge University Press.

Grinstein, F. F. & Fureby, C. 2004 From canonical to complex flows: Recent progress on monotonically integrated LES. *Comp. Sci. Eng.* **6**, 36–49.

Gullbrand, J. & Chow, F. K. 2003 The effect of numerical errors and turbulence models in large-eddy simulations of channel flow, with and without explicit filtering. *J. Fluid Mech.* **495**, 323–341.

Harten, A., Engquist, B., Osher, S. & Chakravarthy, S. 1987 Uniformly high order accurate essentially non-oscillatory schemes, III. *J. Comp. Phys.* **71**, 231–303.

Hickel, S. & Adams, N. 2006*a* Efficient implementation of nonlinear deconvolution

methods for implicit large-eddy simulation. In *Transactions of the Stuttgart High-Performance Computing Center*. Stuttgart, Germany.

Hickel, S. & Adams, N. A. 2006*b* A proposed simplification of the adaptive local deconvolution method. In *Proceedings of CEMRACS 2005*. Marseille, France.

Hickel, S., Adams, N. A. & Domaradzki, J. A. 2006*a* An adaptive local deconvolution method for implicit LES. *J. Comput. Phys.* **213**, 413–436.

Hickel, S., Kempe, T. & Adams, N. 2006*b* Implicit large-eddy simulation applied to turbulent channel flow with periodic constrictions. *Theoret. Comput. Fluid Dynamics* (submitted).

Hickel, S., Kempe, T. & Adams, N. A. 2005 On implicit subgrid-scale modeling in wall-bounded flows. In *Proceedings of the EUROMECH Colloquium 469*, pp. 36–37. Dresden, Germany.

Kravchenko, A. & Moin, P. 1997 On the effect of numerical errors in large-eddy simulation of turbulent flows. *J. Comput. Phys.* **130**, 310–322.

Leonard, A. 1974 Energy cascade in large eddy simulations of turbulent fluid flows. *Adv. Geophys.* **18A**, 237–248.

Lesieur, M. 1997 *Turbulence in Fluids*, 3rd edn. Dordrecht, The Netherlands: Kluwer Academic Publishers.

Moser, R. D., Kim, J. & Mansour, N. 1999 Direct numerical simulation of turbulent channel flow up to $\mathrm{Re}_\tau = 590$. *Phys. Fluids* **11**, 943–945.

Sagaut, P. 2005 *Large-Eddy Simulation for Incompressible Flows*, 3rd edn. Springer.

Schumann, U. 1975 Subgrid scale model for finite-difference simulations of turbulence in plane channels and annuli. *J. Comp. Phys.* **18**, 376–404.

Schwertfirm, F. & Manhart, M. 2006 DNS of passive-scalar transport in turbulent channel flow at high Schmidt numbers. In *Proceedings of Turbulence, Heat and Mass Transfer 5*. (in press).

Yeung, P. K. & Zhou, Y. 1997 On the universality of the Kolmogorov constant in numerical simulations of turbulence. *Tech. Rep.* 97-64. ICASE, NASA Langley Research Center, Hampton, Virginia.